Driving Force Dependent Photoinduced Charge Transfer Dynamics in Polymer-Wrapped Semiconducting Single-Walled Carbon Nanotubes

James A. Alatis, Riley H. Stephenson, Alexander C. Wilcox, Francesco Mastrocinque, Zachary X. W. Widel, George Bullard, Ethan Li, Natalia Rae Alatis, John Naquin, Yusong Bai,[∇] Peng Zhang, David N. Beratan, and Michael J. Therien*

Department of Chemistry, Duke University, Durham, North Carolina, 27708, United States
*Email: michael.therien@duke.edu

ABSTRACT: We investigate the thermodynamic driving-force dependences of photoinduced charge separation (CS) and subsequent charge transfer dynamics in single-walled carbon nanotube (SWNT)–perylenediimide (PDI) donor–acceptor (D–A) superstructures. Pump-probe spectroscopy reveals that $[SWNT^{(\bullet+)n}]$-$(PDI^{-\bullet})_n$ CS states form on an ∼100 fs time scale following photoexcitation; these dynamics are invariant across an ∼400 mV driving force range, indicating that SWNT hole polaron formation time scales are determined by nanotube lattice and solvent relaxation. These CS states feature SWNT hole polarons adjacent to (geminate) and nearby (nongeminate) PDI radical anions. Analysis of the free energy dependence for charge recombination (CR) of $[SWNT^{\bullet+}]^{geminate}$-$(PDI^{-\bullet})$ CS states highlights an ∼2 meV value for D-A electronic coupling (H_{AB}) and ∼0.93 eV for the total reorganization energy (λ_T). A corresponding driving force dependence of the CR dynamics for $([SWNT^{\bullet+}]^{nongeminate}$-$(PDI^{-\bullet})$ CS states indicates a diminished H_{AB} value (∼0.6 meV) and a larger λ_T (∼1.1 eV), consistent with larger transfer distances. SWNT excitons that persist following photoinduced CS drive photooxidation of $PDI^{-\bullet}$ components of $[SWNT^{(\bullet+)n}]$-$(PDI^{-\bullet})_n$ CS states ($^1SWNT^* + PDI^{\bullet-} \rightarrow PDI + SWNT^{\bullet-}$); this reaction manifests a significantly reduced λ_T value (∼0.67 eV) as the initially prepared SWNT reduced state bears the character of a conduction band injected electron ($[SWNT^{\bullet-}]^{CB}$). This reaction thus gives rise to relaxed, nongeminate SWNT electron and hole polarons on the same nanotube; these polarons react on a 10^2 ps time scale independent of the electronic structure of these SWNT-PDI superstructures.

INTRODUCTION

The exceptional optical[1-3] and electronic[4-6] properties of semiconducting single-walled carbon nanotubes (SWNTs) fuel the development of new materials for energy conversion.[7, 8] SWNTs support robust, room-temperature stable excitons with quantized absorption energies covering the ultraviolet-to-near-infrared spectral domain.[5, 9-12] Additionally, optical excitation of s-SWNT donor-acceptor (D-A) systems leads to the formation of both charge transfer states and highly mobile charges.[13-17] In such SWNT D-A assemblies, the mix of photoinduced charge separation (CS), charge migration, and thermal charge recombination (CR) reactions make for complex dynamics. Reactions of CS states with persistent s-SWNT excitons are known to drive the formation of exotic quasiparticles, and to propel further charge transfer reactions, due to the significant excited-state reduction ($^1E^{-/*}$) and excited-state oxidation ($^1E^{*/+}$) potentials of these transient states.[1, 18]

Excited-state dynamical studies illuminate the exceptional scope of light-triggered reactions in carbon nanotube charge transfer systems (**Figure 1**) for SWNT-based molecular D-A hybrid superstructures in which the spatial organization on the nanotube surface and stoichiometry of perylene diimide (PDI) electron acceptors are fixed.[18] SWNT $E_{00} \rightarrow E_{11}$ excitation produces a photoinduced CS state characterized by an initially prepared valence band injected hole (**Figure 1A**). SWNT lattice and solvent nuclear relaxation drive formation of hole polarons (local lattice distortions caused by the positive charges) adjacent to (geminate) and nearby (nongeminate) perylene diimide radical anions. In solution, nanotube hole polarons have delocalization lengths on the order of a few nm.[19] These geminate and nongeminate CS states manifest different CR dynamics;[18] under dilute exciton conditions, the dynamical processes described in **Figure 1A-C** illustrate the scope of light-triggered CS and thermal CR reactions. However, commonly used pulsed laser excitation conditions that trigger photoinduced

electron transfer (ET) reactions in SWNTs generally produce CS states in the presence of excess, unreacted, and highly mobile excitons.[18] **Figure 1D-E** highlights that under conditions in which excess excitons persist following CS, PDI radical anions undergo a multi-body reaction with excess excitons (SWNT $^1E_{11}^*$ + PDI$^{-\bullet}$→ SWNT$^{\bullet-}$ + PDI): this photooxidation reaction enabled by the substantial SWNT exciton excited-state reduction ($^1E^{-/*}$) potential gives rise to a neutral PDI and a SWNT electron polaron (SWNT$^{\bullet-}$). For geminate CS states (**Figure 1D**), the SWNT electron polaron recombines rapidly with a SWNT hole polaron (SWNT$^{\bullet+}$). For nongeminate CS states (**Figure 1E**), the SWNT $^1E_{11}^*$ + PDI$^{-\bullet}$→ SWNT$^{\bullet-}$ + PDI reaction produces more distant SWNT$^{\bullet+}$ and SWNT$^{\bullet-}$ states, which recombine via a mechanism that involves polaron migration.[18]

Here, we elucidate further mechanistic insights for the reactions described detailed in **Figure 1** in closely related SWNT superstructures in which both SWNT and PDI electronic structure are modulated. These excited-state dynamical studies systematically vary the thermodynamic driving forces the reactions indicated in **Figure 1** and shed new light on the nature of light-driven ET reactions in SWNT-based D-A systems.

RESULTS AND DISCUSSION

Figure 1A describes the archetypal *R*-PBN(b)-Ph$_6$-PDI-[(6,5) SWNT] superstructure. In this composition, the *R*-PBN(b)-Ph$_6$ polymer wraps the SWNT surface with a fixed helical pitch (~10 nm) and in a single-handed fashion; because of the nature of the polymer repeat unit, this superstructure features ~4 nm PDI-PDI center-to-center separation distances and ~175 PDI units organized on the length-sorted and 700 nm-long (6,5) SWNT surface.[13, 18, 20-23] **Figure 2A** highlights electronic structural modulation of the parent *R*-PBN(b)-Ph$_6$-PDI polymer derived from PDI bay region substitution.[24-27] Pairing these polymers with either (6,5) or (7,6) SWNTs produces superstructures akin to *R*-PBN(b)-Ph$_6$-PDI-[(6,5) SWNTs], while varying the [SWNT]$^{-/0}$, [SWNT]$^{*/+}$, [PDI]$^{-/0}$, [SWNT]$^{-/*}$, and [SWNT]$^{0/+}$ potentials that characterize these assemblies (**Figure 2B**). These *R*-PBN(b)-Ph$_6$-PDI-[(7,6) SWNT], *R*-PBN(b)-Ph$_6$-(Ph(CF$_3$)$_2$)$_2$-PDI-[(7,6) SWNT], *R*-PBN(b)-Ph$_6$-PDI-[(6,5) SWNT], *R*-PBN(b)-Ph$_6$-(OPh)$_2$-PDI-[(6,5) SWNT], and *R*-PBN(b)-Ph$_6$-(Ph(CF$_3$)$_2$)$_2$-PDI-[(6,5) SWNT] superstructures modulate the thermodynamic driving forces for ultrafast CS, thermal CR reaction, and persistent exciton driven PDI radical anion photooxidation triggered upon SWNT E_{00}→E_{11} excitation. Femtosecond pump-probe transient absorption spectroscopy experiments were performed using excitation fluences that produce initially prepared SWNT exciton densities of ~4 and ~10 excitons per 100 nm.[18]

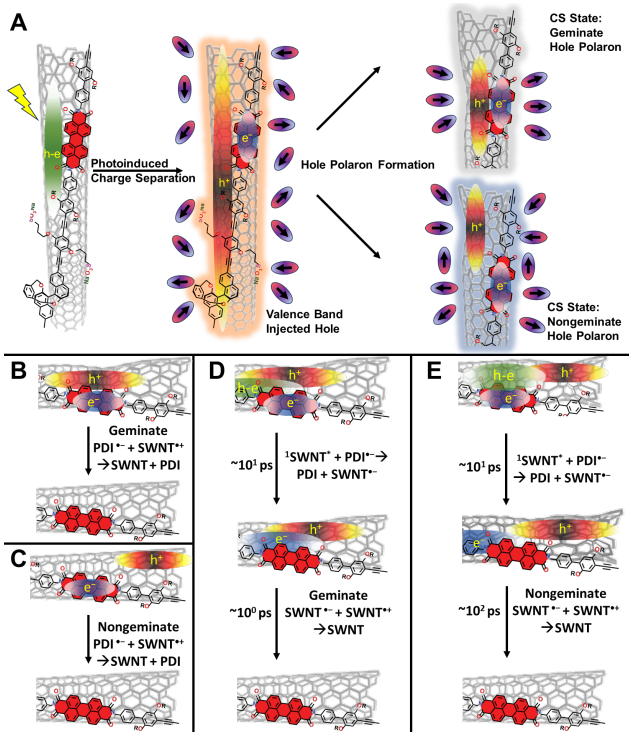

Figure 1. *R* Schematic illustration of (**A**) exciton generation, light-triggered formation of the initially prepared charge separated (CS) state, and subsequent polaron formation dynamics that give rise to CS states characterized by SWNT hole polarons both geminate and nongeminate to a PDI$^{-\bullet}$.[18] (**B-C**) Thermal charge recombination (CR) reactions and (**D-E**) multibody processes that promote additional charge transfer (CT) reactions characterized in the benchmark *R*-PBN(b)-Ph$_6$-PDI-[(6,5) SWNT] superstructure. Under low excitation fluences that produce dilute (<4 excitons per 100 nm) exciton concentrations (**B**) geminate CS states exhibit ~10^1 ps time scale thermal CR dynamics, while (**C**) nongeminate CS states manifest thermal CR on an ~10^2 ps time scale.[18] As excitation fluence is increased into a regime (> 8 excitons per 100 nm) where SWNT excitons persist following light-triggered CS (**D-E**), a multi-body driven CT reaction—exciton driven PDI radical anion photooxidation—becomes important. (**D**) For geminate CS states, SWNT E_{11} excitons mediate a decay channel for the PDI$^{-\bullet}$ population that is reflected as a fast (~10^1 ps) decay of the PDI$^{-\bullet}$→PDI^{-*} transient absorptive signal, producing a SWNT electron polaron (SWNT$^{\bullet-}$), which recombines rapidly (< 1 ps) with its geminate SWNT hole polaron (SWNT$^{\bullet+}$) partner.[18] (**E**) When excess excitons react with nongeminate CS states, this multi-body interaction also causes the decay of the transient PDI$^{-\bullet}$ signal on the 10^1 ps time scale, but instead produces a SWNT electron polaron nongeminate to a SWNT hole polaron; CR dynamics of these nongeminate SWNT$^{\bullet-}$ and SWNT$^{\bullet+}$ states occur on the order of 10^2 ps.[18]

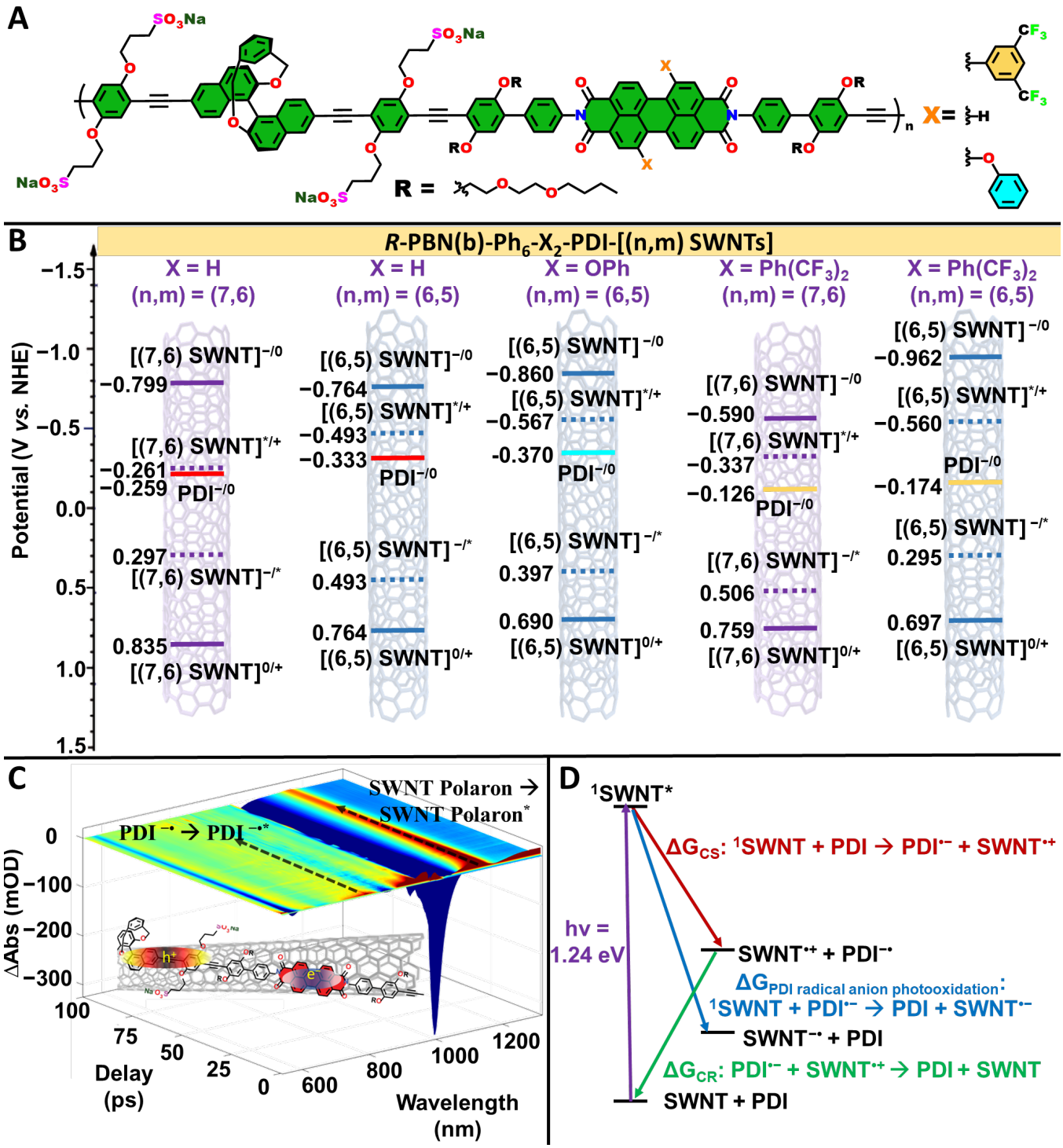

Figure 2. (A) Structure of *R*-PBN(b)-Ph$_6$-X$_2$-PDI polymers; X denotes the PDI bay region substituent (X = OPh, teal; X = H, black; X = Ph(CF$_3$)$_2$, orange). (B) Ground- and excited-state redox potentials of isolated and characterized polymer-wrapped SWNT superstructures. (C) Representative three-dimensional transient absorbance spectra of *R*-PBN(b)-(OPh)$_2$-PDI-[(6,5) SWNTs] highlighting the respective PDI radical anion and SWNT polaron transient absorbative spectroscopic signatures at 780 and 1160 nm, observed following SWNT E_{00}→E_{11} photoexcitation (1000 nm).[13, 18, 23] The inset illustrates the PDI radical anion and the SWNT hole polaron states that are spectroscopically monitored. (D) Energy level diagram depicting thermodynamic driving forces for photoinduced CS, thermal CR, and persistent SWNT E_{11} exciton driven PDI radical anion photooxidation for the *R*-PBN(b)-(OPh)$_2$-PDI-[(6,5) SWNT system. Photoinduced charge separation (red arrow) produces CS states characterized by a SWNT hole polaron and a PDI radical anion. These CS states can either undergo a thermal charge recombination reaction (green arrow) or can react through a multibody mediated process in which excess excitons drive PDI radical anion photooxidation and produce a SWNT electron polaron (SWNT $^1E_{11}{}^*$ + PDI$^{-\bullet}$→ SWNT$^{\bullet-}$ + PDI, blue arrow).

PHOTOINDUCED CHARGE SEPERATION

Under an excitation fluence that prepares an initial exciton density of ~4 excitons per 100 nm, ultrafast CS reactions consume the exciton population ([SWNT $^1E_{11}^*$]-(PDI) → [SWNT$^{(\bullet+)n}$]-(PDI$^{-\bullet}$)$_n$) (**Figure 1A**).[13, 18] The respective transient absorptive signatures of the PDI radical anion and the SWNT hole polaron allow each component of these ([SWNT$^{(\bullet+)n}$]-(PDI$^{-\bullet}$)$_n$ CS states that are prepared following SWNT E_{00}→E_{11} excitation to be tracked independently.[18] In this light-triggered reaction, the initially prepared CS state features a SWNT valence band hole ([SWNT$^{(\bullet+)n}$]^{VB}; **Figure 3A**). On a ~100 fs time scale, nanotube lattice relaxation coupled with sub-ps time scale solvent polarization produces SWNT hole polarons ([SWNT$^{(\bullet+)n}$]^{VB}-(PDI$^{-\bullet}$)$_n$ → [SWNT$^{(\bullet+)n}$]-(PDI$^{-\bullet}$)$_n$).[18] Since only the relaxed polaron is spectroscopically observable, light-triggered CS dynamics (k_{CS}) display no apparent driving force dependence (1.38×10^{12} s^{-1} < k_{CS} < 2.31×10^{12} s^{-1}) over the ~400 mV driving force range probed in these experiments (**Figure 3B**). Consistent with this model, the rise time of the PDI radical anion is approximately 5-fold faster than that of the SWNT polaron, but convoluted with the instrument response function (Supporting Information, pp. S74-83).

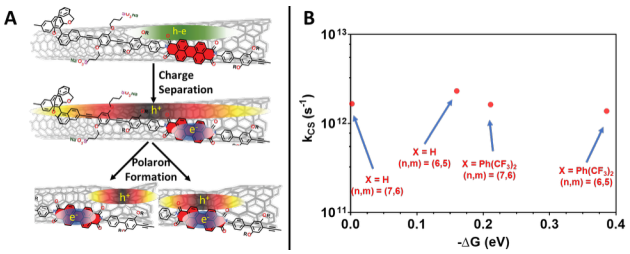

Figure 3. (A) Schematic depiction of the initially prepared photoinduced charge separated states ([SWNT $^1E_{11}^*$]-(PDI) → [SWNT$^{(\bullet+)n}$]^{VB}-(PDI$^{-\bullet}$)$_n$) and the subsequent nuclear and solvent relaxation dynamics that give rise to formation of relaxed hole polarons [SWNT$^{(\bullet+)n}$]^{VB}-(PDI$^{-\bullet}$)$_n$ → [SWNT$^{(\bullet+)n}$]-(PDI$^{-\bullet}$)$_n$) on a ~10^{-1} ps timescale.These relaxation dynamics result in CS states in which the nanotube hole polaron is either geminate or nongeminate to a PDI$^{-\bullet}$. (B) Thermodynamic driving force dependence of the charge separation rate constant (k_{CS}), indicating that the observed dynamics reflect near-uniform polaron formation time scales.

THERMAL CHARGE RECOMBINATION OF GEMINATE SWNT HOLE POLARONS AND PDI RADICAL ANIONS

Geminate CS states (**Figure 3A**, bottom right) and nongeminate CS states (**Figure 3A**, bottom left) are produced in near-equal populations under reaction conditions in which SWNT E_{11} excitons are dilute (~4 excitons per 100 nm); thermal charge recombination of these geminate and nongeminate CS states may be distinguished dynamically.[18] CR of geminate ([SWNT$^{(\bullet+)n}$]-(PDI$^{-\bullet}$)$_n$) CS states (**Figure 4A**) displays a driving force dependent CR rate constant ($k_{CR}^{geminate}$) that can be modulated over two orders of magnitude (2.97×10^{10} s^{-1} < $k_{CR}^{geminate}$ < 1.70×10^{11} s^{-1}) for the compositions described in **Figure 2B**. **Figure 4B**, which plots $k_{CR}^{geminate}$ as a function of thermodynamic driving force, suggests a total reorganization energy (λ_T) of ~1 eV for this reaction. The SWNT inner sphere reorganization energy is small (λ_i < 100 meV) due to the high symmetry, rigid nature, and electronic band structures of these compositions which make possible substantial charge (polaron) delocalization lengths.[1, 3, 15, 19] The magnitude of the evaluated λ_T is thus congruent with classical electrostatic dielectric continuum model calculations that determine that λ_T is dominated by an outer sphere reorganization energy (λ_o) contribution of ~1.0 eV for this CR process (Supporting Information, pp. S85-86). The **Figure 4B** data thus demonstrate that CR of geminate PDI$^{\bullet-}$/SWNT$^{\bullet+}$ CS states (**Figure 4A**) occurs through an uncomplicated ET mechanism that is described by semi-classical Marcus theory.[28, 29]

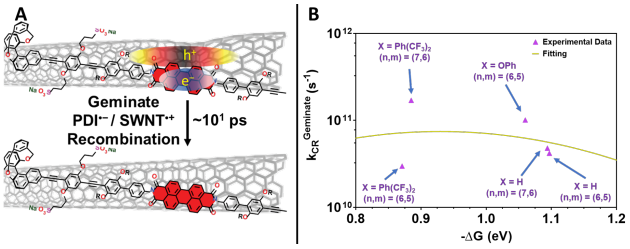

Figure 4: (A) Depiction of a thermal CR reaction for a geminate PDI radical anion/SWNT hole polaron CS state. (B) Thermodynamic driving force dependence of the geminate CR ([SWNT$^{\bullet+}$]^{geminate}-(PDI$^{-\bullet}$) → SWNT + PDI) reaction rate constant ($k_{CR}^{geminate}$) magnitude. A nonlinear regression to the Marcus equation (Supporting Information, pp. S88-90) provides insight into the magnitude of electronic coupling (H_{AB} ~2 meV) and the total reorganization energy (λ_T ~0.93 eV).

THERMAL CHARGE RECOMBINATION OF NONGEMINATE SWNT HOLE POLARONS AND PDI RADICAL ANIONS

The thermal CR time scale for nongeminate [SWNT$^{(\bullet+)n}$]-(PDI$^{-\bullet}$)$_n$ CS states (~10^2 ps) evaluated under reaction conditions in which SWNT E_{11} exciton reactants are dilute (~4 excitons per 100 nm) (**Figure 5**) is approximately an order of magnitude longer than the time scale determined for geminate [SWNT$^{(\bullet+)n}$]-(PDI$^{-\bullet}$)$_n$ charge separated states (**Figure 4B**); these differences derive from the distance dependences of the D-A electronic coupling and the reaction reorganization energy. The data shown in **Figure 5B** highlight the relatively weak thermodynamic driving force dependence of thermal CR for nongeminate CS states (2.33×10^9 s^{-1} < $k_{CR}^{nongeminate}$ < 1.41×10^{10} s^{-1}), relative to that found for thermal CR of geminate CS states (**Figure 4B)**. Factors that likely contribute to the observed soft dependence of $k_{CR}^{nongeminate}$ on thermodynamic driving force include the nature of the s-SWNT valence band structure[1, 3, 19, 30, 31] and the fact that nongeminate [SWNT$^{(\bullet+)n}$]-(PDI$^{-\bullet}$)$_n$ CS states manifest heterogeneity with respect to their CR distances. This CR distance heterogeneity causes the magnitudes of D-A electronic coupling and the associated reorganization energies for these CR reactions to be nonuniform. Results from dielectric continuum model calculations (**Figure 5C**) find that small variations in PDI radical anion to SWNT hole polaron distances change the magnitude of the reorganization energy over an ~0.3 eV range.

Computational data (Supporting Information, pp. S88-90) summarized in **Figure 5C-D** suggest that the driving force dependence shown in **Figure 5B** for nongeminate [SWNT$^{(\bullet+)n}$]-(PDI$^{-\bullet}$)$_n$ CS states derives from Marcus normal region behavior over driving forces near the barrierless point.

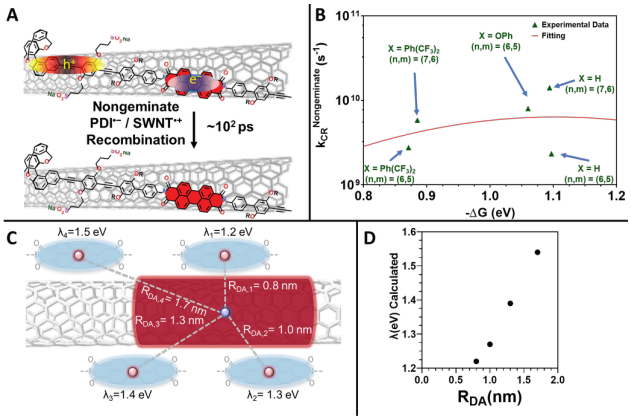

Figure 5: (A) Depiction of the thermal charge recombination reaction involving a PDI radical anion and a nongeminate SWNT hole polaron ([SWNT$^{\bullet+}$]^{nongeminate}-(PDI$^{-\bullet}$) → SWNT + PDI). (B) Thermodynamic driving force dependence of the nongeminate charge recombination rate constant ($k_{CR}^{nongeminate}$) magnitude. The nonlinear regression to the Marcus equation provides insight into the magnitude of the effective electronic coupling (H_{AB} ~0.6 meV) and the total effective reorganization energy (λ_T ~1.1 eV). (C) Schematic depiction of results obtained from classical electrostatic continuum model calculations (Supporting Information, pp. S85-87) that assess the impact of donor (PDI$^{-\bullet}$) to acceptor (SWNT$^{\bullet+}$) center-to-center distance (R_{DA}) in nongeminate [SWNT$^{(\bullet+)n}$]-(PDI$^{-\bullet}$)$_n$ CS states upon the extent of the reorganization energy (λ). (D) Graphical representation of the dependence of λ on R_{DA} for thermal CR of nongeminate [SWNT$^{(\bullet+)n}$]-(PDI$^{-\bullet}$)$_n$ CS states.

PHOTOINDUCED OXIDATION OF PDI RADICAL ANIONS BY SWNT SINGLET EXCITONS

When excitation fluences prepare initial exciton densities exceeding 4 per (100 nm), excitons persist (**Figure 1D-E**) after ultrafast CS (**Figure 3A**).[18] The substantial $^1E^{-/*}$ potential of these SWNT singlet E_{11} excitons drives photooxidation PDI radical anions. This multi-body reaction involving an excess, persistent exciton and a PDI radical anion produces a reduced SWNT state (SWNT $^1E_{11}^*$ + PDI$^{-\bullet}$→ SWNT E_{00}^- + PDI) (**Figure 1 D-E**).[18] **Figure 6A** illustrates this E_{11} exciton-driven PDI$^{-\bullet}$ photooxidation reaction acquired under photoexcitation conditions that produce ~10 excitons per 100 nm for these 700 nm-long polymer-wrapped SWNT superstructures. Importantly, when excess excitons are present, the photooxidation of PDI radical anions for both geminate and nongeminate CS states occurs at an identical rate for a given *R*-PBN(b)-Ph$_6$-X$_2$-PDI-[(n,m) SWNT] superstructure. Over the driving force range noted in **Figure 6B**, the rate constant ($k_{PDI\ radical\ anion\ photooxidation}$) for the SWNT $^1E_{11}^*$ + PDI$^{-\bullet}$→ SWNT E_{00}^- + PDI reaction is modulated over two orders of magnitude ($3.17 \times 10^{10} < k_{PDI\ radical\ anion\ photooxidation} < 1.90 \times 10^{11}$ s^{-1}). These studies indicate a reorganization energy of ~0.67 eV for this reaction, much smaller than that observed for CR of geminate [SWNT$^{(\bullet+)n}$]-(PDI$^{-\bullet}$)$_n$ CS states (**Figure 4**).

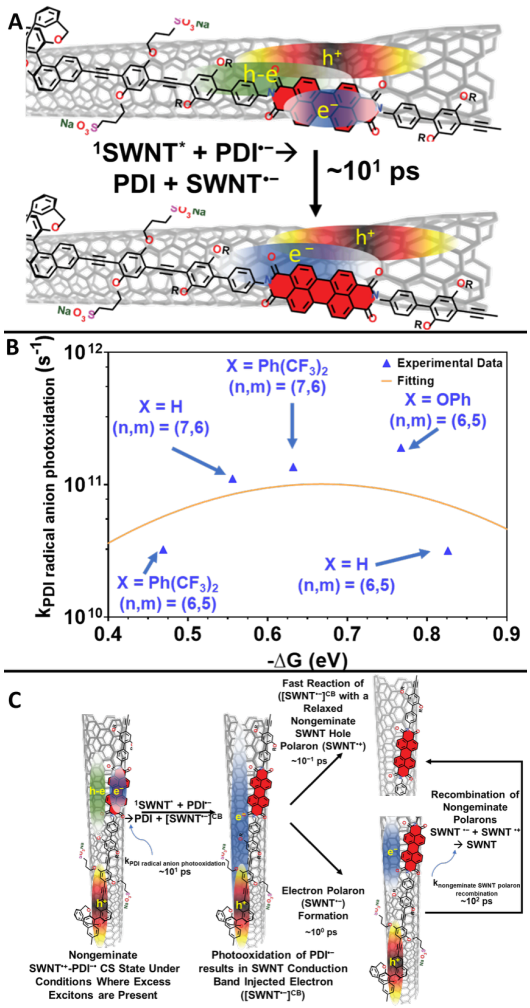

Figure 6: (A) Schematic depiction of photoinduced oxidation of a PDI radical anion in a (SWNT$^{\bullet+}$)-(PDI$^{-\bullet}$) CS state through a multibody reaction with a SWNT exciton (^{1}SWNT* + PDI$^{\bullet-}$ → PDI + SWNT$^{\bullet-}$).This process occurs on the ~10^1 ps timescale when excitons persist following charge separation. (B) Thermodynamic driving force dependence of the rate constant for SWNT $^1E_{11}$ exciton photooxidation of the PDI radical anion ($k_{PDI\ radical\ anion\ photooxidation}$). A nonlinear regression to the Marcus equation provides insight into the magnitude of the effective electronic coupling (H_{AB} ~2 meV) and the total effective reorganization energy (λ_T ~0.67 eV). A similar analysis using the Jortner equation is described in the Supporting Information. (C, *left, center*) Image highlighting that photooxidation of a PDI radical anion results in an initially formed SWNT E_{00}^- state that is best described as a conduction band injected electron (^{1}SWNT* + PDI$^{\bullet-}$ → PDI + [SWNT$^{\bullet-}$]^{CB}). Because of its unrelaxed and delocalized nature, the [SWNT$^{\bullet-}$]^{CB} state can undergo fast (~10^{-1} ps) charge recombination with a nongeminate SWNT hole polaron; excited-state dynamical data indicate ~10% of the hole polarons associated with nongeminate (SWNT$^{\bullet+}$)-(PDI$^{-\bullet}$) CS states are consumed in such a reaction (Supporting Information, pp. S91-92). (C, *right*) Lattice and solvent relaxation dynamics convert remaining [SWNT$^{\bullet-}$]^{CB} states to SWNT electron polarons on an ultrafast time scale, which can form anywhere along the nanotube framework. Charge

recombination of nongeminate SWNT electron and hole polarons ($SWNT^{\bullet+}$ + $SWNT^{\bullet-}$ → SWNT) occurs on an ~10^2 ps time scale.

The thermodynamic driving force dependence of the $k_{PDI\ radical\ anion\ photooxidation}$ rate constant magnitude chronicled in the **Figure 6B** data thus indicates an increased delocalization length for the initially prepared, unrelaxed SWNT E_{00}^{-} state that is instantly formed following PDI radical anion photooxidation relative to that for the relaxed SWNT hole polaron component of the CS state (**Figure 6C**, *left, center*). Analogous to the valence band injected hole ($[SWNT^{\bullet+}]^{VB}$) depicted in **Figure 1A** and **Figure 3A**,[18] this initially prepared SWNT E_{00}^{-} state, formed upon PDI radical anion photooxidation, bears the character of a conduction band injected electron ($[SWNT^{\bullet-}]^{CB}$); sub-ps SWNT lattice and solvational relaxation dynamics result in SWNT electron polaron formation ($[SWNT^{\bullet-}]^{CB}$ → $SWNT^{\bullet-}$). A consequence of this SWNT E_{11} exciton driven photooxidation reaction ($^1SWNT^*$ + $PDI^{\bullet-}$ → PDI + $[SWNT^{\bullet-}]^{CB}$) that initially produces a $[SWNT^{\bullet-}]^{CB}$ state with augmented electronic delocalization compared to that of the relaxed SWNT electron polaron state ($SWNT^{\bullet-}$) is that a new decay channel opens for $SWNT^{\bullet+}$ components of nongeminate $[SWNT^{(\bullet+)n}]$-$(PDI^{-\bullet})_n$ CS states on the ultrafast time domain (**Figure 6C**, *left, center*). For the excitation conditions described in **Figure 6A**, consistent with previously published data, the reaction trajectory enabled by the $[SWNT^{\bullet-}]^{CB}$ state consumes ~10% of the hole polarons associated with nongeminate ($SWNT^{\bullet+}$)-($PDI^{-\bullet}$) CS states (Supporting Information, pp. S91-92).[18] The recombination dynamics of these nongeminate SWNT hole and electron polarons ($k^{nongeminate}_{polaron\ recombination}$) occurs on an ~$10^2$ ps time scale (**Figure 6C**, *right*).

THERMAL CHARGE RECOMBINATION OF NONGEMINATE SWNT HOLE AND ELECTRON POLARONS

The diffusion controlled recombination dynamics of nongeminate $SWNT^{\bullet+}$ and $SWNT^{\bullet-}$ charge carriers should not depend strongly upon *R*-PBN(b)-Ph_6-X_2-PDI-[(n,m) SWNT] electronic structure as $SWNT^{-/0}$ and $SWNT^{0/+}$ potentials differ markedly from the corresponding one-electron reduction and oxidation potentials of the respective polymers that wrap the SWNT surface (**Figure 2B**). Indeed, the evaluated rate constants for nongeminate CR ($k^{nongeminate}_{polaron\ recombination}$) are near uniform in these *R*-PBN(b)-Ph_6-X_2-PDI-[(n,m) SWNT] superstructures ($2.3 \times 10^9\ s^{-1} < k^{nongeminate}_{polaron\ recombination} < 4.8 \times 10^9\ s^{-1}$) (**Figure 7**), congruent with this expectation. The data in **Figure 7C**, which describes the SWNT polaron population over the 100 - 1000 ps time domain, highlights the uniform nature of these decay dynamics in these *R*-PBN(b)-Ph_6-X_2-PDI-[(n,m) SWNT] systems.

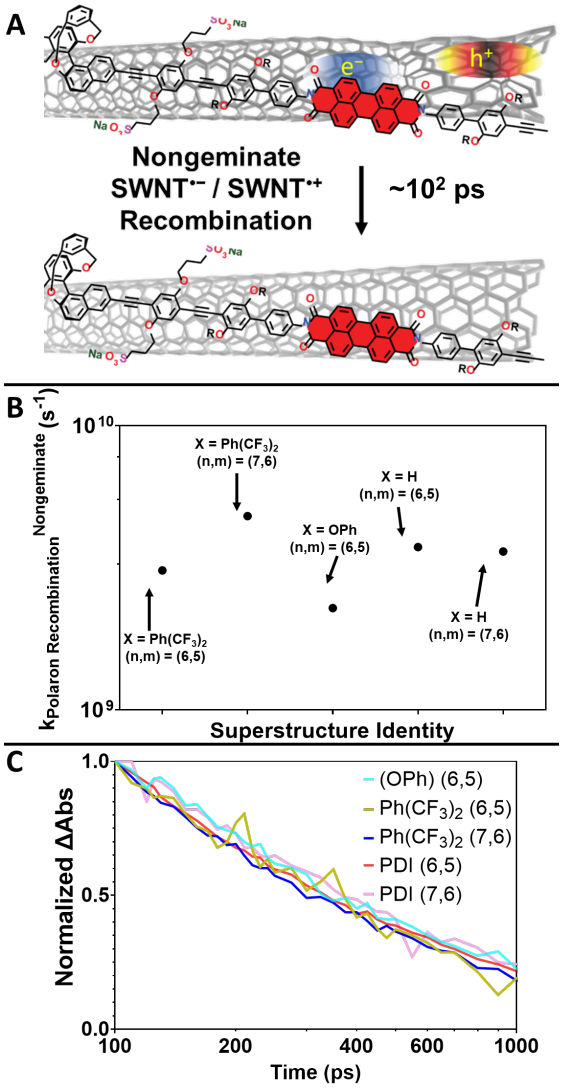

Figure 7: (A) Schematic depiction of thermal charge recombination of nongeminate SWNT hole and electron polarons ($SWNT^{\bullet+}$ + $SWNT^{\bullet-}$ → $SWNT^0$)following SWNT $^1E_{11}$ exciton photooxidation of the PDI radical anion components (**Figure 6C**) of nongeminate PDI radical anion/SWNT hole polaron CS states (**Fig. 5**) under experimental conditions in which excess excitons are present. (B) Rate constants determined for thermal charge recombination between nongeminate SWNT polarons ($k^{nongeminate}_{polaron\ recombination}$) for each polymer-wrapped SWNT superstructure. The driving force for this process is determined by the $SWNT^{-/0}$ and $SWNT^{0/+}$ potentials. (C) Population of SWNT polarons as a function of time; note that the rate at which nongeminate polarons are consumed is not correlated with the *R*-PBN(b)-Ph_6-X_2-PDI-[(n,m) SWNT] electronic structure (**Figure 2B**).

CONCLUSIONS

Optical excitation of (D-A) systems constructed with single-walled carbon nanotubes support a diverse set of charge-transfer reactions. *R*-PBN(b)-Ph_6-X_2-PDI-[(n,m) SWNT] superstructures, which fix perylenediimide electron acceptors in van der Waals contact on the carbon nanotube surface at 4 nm intervals due to the single-handed uniform wrapping of the polymer about the nanotube at fixed helical pitch (~10 nm), are well-defined assemblies in which the SWNT and PDI electronic structures may be modulated systematically. Light-triggered charge separation (CS) reactions were interrogated in these assemblies, which demonstrated that $[SWNT^{(\bullet+)n}]$-$(PDI^{-\bullet})_n$ CS states are produced on an ~100 fs time scale. The lack of discernable driving force dependence for these reactions is consistent with the rise time of the SWNT hole polaron ($SWNT^{\bullet+}$) signal being determined by ultrafast nanotube lattice relaxation solvent polarization dynamics. These CS states formed on the ultrafast time scale feature SWNT hole polarons adjacent to (geminate) and nearby (nongeminate) perylenediimide radical anions. The thermodynamic driving force dependence of the thermal charge recombination (CR) rate constant for $[SWNT^{\bullet+}]^{geminate}$-$(PDI^{-\bullet})$ CS states indicates that the electronic coupling magnitude and the total reorganization energy for the $[SWNT^{\bullet+}]^{geminate}$-$(PDI^{-\bullet})$ → SWNT + PDI reaction are ~2 meV and ~0.93 eV, respectively. Consistent with the larger separation of the $SWNT^{\bullet+}$ and $PDI^{-\bullet}$ charges in the nongeminate CS states, the magnitude of the computed coupling (~0.6 meV) is reduced while that for λ_T (~1.1 eV) is larger for the for the $[SWNT^{\bullet+}]^{nongeminate}$-$(PDI^{-\bullet})$ → SWNT + PDI reaction than that observed for the analogous CR reaction for geminate CS states.

In these *R*-PBN(b)-Ph_6-X_2-PDI-[(n,m) SWNT] systems, the substantial excited-state reduction ($^1E^{-/*}$) potential of persistent SWNT excitons drives photooxidation of $PDI^{-\bullet}$ components of $[SWNT^{(\bullet+)n}]$-$(PDI^{-\bullet})_n$ CS states ($^1SWNT^*$ + $PDI^{\bullet-}$ → PDI + $SWNT^{\bullet-}$). Excitation fluence and thermodynamic driving force dependence studies of the rate constant for SWNT $^1E_{11}$ exciton photooxidation of the PDI radical anion ($k_{PDI\ radical\ anion\ photooxidation}$) show the following remarkable features: (i) a dramatically reduced effective total reorganization energy (λ_T ~0.67 eV) for this reaction relative to reorganization energies evaluated for CS state thermal CR, and (ii) ~10% of the nanotube hole polarons associated with nongeminate ($SWNT^{\bullet+}$)-($PDI^{-\bullet}$) CS states are consumed on an ultrafast (~100 fs) time scale. Taken together, these results indicate that the initially prepared SWNT reduced state formed upon PDI radical anion photooxidation has the features of a conduction band injected electron ($[SWNT^{\bullet-}]^{CB}$), a more delocalized state than the relaxed carbon nanotube electron polaron ($SWNT^{\bullet-}$). Given the magnitude of exciton diffusion constant (~0.9 cm^2s^{-1}) in SWNTS,[1] these data thus underscore that studies that examine photoinduced CS reactions involving SWNTs must consider potential reaction trajectories of CS states that are prepared in the presence of excess, unreacted, and highly mobile excitons.

Nanotube $^1E_{11}$ exciton photooxidation of reduced electron acceptor components of $([SWNT^{\bullet+}]^{nongeminate}$-$(PDI^{-\bullet})$ CS states thus give rise to SWNT electron polarons that have nongeminate spatial arrangements with SWNT hole polarons that trace their genesis to the ultrafast photoinduced CS reaction. The dynamics of thermal charge recombination of these nongeminate SWNT hole and electron polarons ($SWNT^{\bullet+}$ + $SWNT^{\bullet-}$ → $SWNT^0$) occur on an ~10^2 ps time scale and is independent of *R*-PBN(b)-Ph_6-X_2-PDI-[(n,m) SWNT] electronic structure.

A distinct advantage of these *R*-PBN(b)-Ph_6-X_2-PDI-[(n,m) SWNT] systems is that they organize on the order of a few hundred equally separated PDI units on a length-sorted ~700 nm-long carbon nanotube surface, allowing each component of the light-triggered CS reaction to be independently tracked spectroscopically in a straightforward manner. Because SWNT hole and electron polarons have identical masses, their electronic absorptions are coincident.[32] These experiments thus underscore the fact that measured SWNT polaron lifetimes do not necessarily correlate with the lifetimes of CS states formed through a light-triggered $[SWNT\ ^1E_{11}^*]$-(Acceptor) → $[SWNT^{(\bullet+)n}]$-$(Acceptor^{-\bullet})_n$ reaction, as the decay of the transient polaron absorption signal can also reflect the timescale for the reaction of oppositely charged $SWNT^{\bullet-}$ and $SWNT^{\bullet+}$ polarons in a single carbon nanotube.

ASSOCIATED CONTENT

Supporting Information. Synthetic procedures, characterization data (^1H NMR, GPC, CV, and UV-Vis-NIR EAS), sample preparation details, additional transient spectroscopic experimental data, exciton density calculations, and details regarding computational methods. This material is available free of charge via the Internet at http://pubs.acs.org.

AUTHOR INFORMATION

Corresponding Author

* Michael Therien — **Department of Chemistry, Duke University, Durham, North Carolina, 27708, United States.**
orcid.org/0000-0003-4876-0036
Email: michael.therien@duke.edu

Authors

James A. Alatis — **Department of Chemistry, Duke University, Durham, North Carolina, 27708, United States.**
orcid.org/0000-0003-2585-1103

Riley H. Stephenson — **Department of Chemistry, Duke University, Durham, North Carolina, 27708, United States.**
orcid.org/0000-0003-3419-9241

Alexander C. Wilcox — **Department of Chemistry, Duke University, Durham, North Carolina, 27708, United States.**
orcid.org/0009-0007-0985-161X

Francesco Mastrocinque — **Department of Chemistry, Duke University, Durham, North Carolina, 27708, United States.**
orcid.org/0000-0002-5945-4045

Zachary X. W. Widel – **Department of Chemistry, Duke University, Durham, North Carolina, 27708, United States. orcid.org/**0000-0003-3550-4498

George Bullard – **Department of Chemistry, Duke University, Durham, North Carolina, 27708, United States. orcid.org/**0000-0002-3725-9046

Ethan Li – **Department of Chemistry, Duke University, Durham, North Carolina, 27708, United States. orcid.org/**0009-0003-9392-9168

Natalia Rae Alatis – **Department of Chemistry, Duke University, Durham, North Carolina, 27708, United States. orcid.org/**0009-0009-9158-4665

John Naquin – **Department of Chemistry, Duke University, Durham, North Carolina, 27708, United States. orcid.org/**0009-0006-6366-5079

Yusong Bai – **Department of Chemistry, Brown University, Providence, Rhode Island, 02912, United States. orcid.org/**0000-0001-6097-6409

Peng Zhang – **Department of Chemistry, Duke University, Durham, North Carolina, 27708, United States. orcid.org/**0000-0003-2623-4115

David N. Beratan – **Department of Chemistry, Duke University, Durham, North Carolina, 27708, United States. orcid.org/**0000-0003-4758-8676

Present Addresses

∇Department of Chemistry, Brown University, Providence, Rhode Island, 02912, United States.

Author Contributions

All authors have given approval to the final version of the manuscript.

ACKNOWLEDGMENT

This work was funded by the Division of Chemical Sciences, Geosciences, and Biosciences, Office of Basic Energy Sciences, of the U.S. Department of Energy (DOE) through Grant DESC0001517 to MJT and DESC0019400 to DNB. The authors also acknowledge the DOE and the Air Force Office of Scientific Research (FA9550-20-1-0121) for research infrastructure enabling transient dynamical spectroscopic experiments. J.A.A., R.H.S., F.M., and Z.X.W.W. thank Duke University for Graduate Program Nanoscience Fellowships; Y.B. and G. B. gratefully acknowledge the Fitzpatrick Institute of Photonics at Duke University for John T. Chambers Scholars Awards. The authors are grateful to Dr. Jeffrey A. Fagan and Dr. Ming Zheng (National Institute of Standards and Technology) for providing guidance and support regarding aqueous two-phase extraction-based purification methods for surfactant-dispersed single-wall carbon nanotubes.

Notes

The authors declare no competing financial interest.

REFERENCES

(1) Bai, Y.; Olivier, J.-H.; Bullard, G.; Liu, C.; Therien, M. J., Dynamics of charged excitons in electronically and morphologically homogeneous single-walled carbon nanotubes. *Proc. Natl. Acad. Sci. U.S.A.* **2018**, *115*, 674-679.

(2) Bachilo, S. M.; Strano, M. S.; Kittrell, C.; Hauge, R. H.; Smalley, R. E.; Weisman, R. B., Structure-Assigned Optical Spectra of Single-Walled Carbon Nanotubes. *Science* **2002**, *298*, 2361-2366.

(3) Avouris, P.; Freitag, M.; Perebeinos, V., Carbon-nanotube photonics and optoelectronics. *Nat. Photonics* **2008**, *2*, 341-350.

(4) Bockrath, M.; Cobden, D. H.; McEuen, P. L.; Chopra, N. G.; Zettl, A.; Thess, A.; Smalley, R. E., Single-Electron Transport in Ropes of Carbon Nanotubes. *Science* **1997**, *275*, 1922-1925.

(5) Avouris, P.; Chen, Z.; Perebeinos, V., Carbon-based electronics. *Nat. Nanotechnol.* **2007**, *2*, 605-615.

(6) Islam, A. E.; Rogers, J. A.; Alam, M. A., Recent Progress in Obtaining Semiconducting Single-Walled Carbon Nanotubes for Transistor Applications. *Adv. Mater.* **2015**, *27*, 7908-7937.

(7) Arnold, M. S.; Blackburn, J. L.; Crochet, J. J.; Doorn, S. K.; Duque, J. G.; Mohite, A.; Telg, H., Recent developments in the photophysics of single-walled carbon nanotubes for their use as active and passive material elements in thin film photovoltaics. *Phys. Chem. Chem. Phys.* **2013**, *15*, 14896-14918.

(8) Bindl, D. J.; Wu, M. Y.; Prehn, F. C.; Arnold, M. S., Efficiently harvesting excitons from electronic type-controlled semiconducting carbon nanotube films. *Nano Lett.* **2011**, *11*, 455-60.

(9) Blackburn, J. L., Semiconducting Single-Walled Carbon Nanotubes in Solar Energy Harvesting. *ACS Energy Lett.* **2017**, *2*, 1598-1613.

(10) Bindl, D. J.; Safron, N. S.; Arnold, M. S., Dissociating Excitons Photogenerated in Semiconducting Carbon Nanotubes at Polymeric Photovoltaic Heterojunction Interfaces. *ACS Nano* **2010**, *4*, 5657-5664.

(11) Lüer, L.; Hoseinkhani, S.; Polli, D.; Crochet, J.; Hertel, T.; Lanzani, G. *Exciton size and mobility in (6,5) single-walled carbon nanotubes*; SPIE, 2008.

(12) Weisman, R. B.; Bachilo, S. M., Dependence of Optical Transition Energies on Structure for Single-Walled Carbon Nanotubes in Aqueous Suspension: An Empirical Kataura Plot. *Nano Lett.* **2003**, *3*, 1235-1238.

(13) Olivier, J.-H.; Park, J.; Deria, P.; Rawson, J.; Bai, Y.; Kumbhar, A. S.; Therien, M. J., Unambiguous Diagnosis of Photoinduced Charge Carrier Signatures in a Stoichiometrically Controlled Semiconducting Polymer-Wrapped Carbon Nanotube Assembly. *Angew. Chem. Int. Ed.* **2015**, *54*, 8133-8138.

(14) Kuang, Z.; Berger, F. J.; Lustres, J. L. P.; Wollscheid, N.; Li, H.; Lüttgens, J.; Leinen, M. B.; Flavel, B. S.; Zaumseil, J.; Buckup, T., Charge Transfer from Photoexcited Semiconducting Single-Walled Carbon Nanotubes to Wide-Bandgap Wrapping Polymer. *J. Phys. Chem. C* **2021**, *125*, 8125-8136.

(15) Ihly, R.; Mistry, K. S.; Ferguson, A. J.; Clikeman, T. T.; Larson, B. W.; Reid, O.; Boltalina, O. V.; Strauss, S. H.; Rumbles, G.; Blackburn, J. L., Tuning the driving force for exciton dissociation in single-walled carbon nanotube heterojunctions. *Nat. Chem.* **2016**, *8*, 603-609.

(16) Ehli, C.; Oelsner, C.; Guldi, D. M.; Mateo-Alonso, A.; Prato, M.; Schmidt, C.; Backes, C.; Hauke, F.; Hirsch, A., Manipulating single-wall carbon nanotubes by chemical doping and charge transfer with perylene dyes. *Nat. Chem.* **2009**, *1*, 243-249.

(17) Long, R.; Prezhdo, O. V., Asymmetry in the Electron and Hole Transfer at a Polymer–Carbon Nanotube Heterojunction. *Nano Lett.* **2014**, *14*, 3335-3341.

(18) Widel, Z. X. W.; Alatis, J. A.; Stephenson, R. H.; Mastrocinque, F.; Wilcox, A. C.; Bullard, G.; Olivier, J.-H.; Bai, Y.; Zhang, P.; Beratan, D.; Therien, M. J., Fluence Dependent

Photoinduced Charge Transfer Dynamics in Polymer-Wrapped Semiconducting Single-Walled Carbon Nanotubes. *J. Am. Chem. Soc.* **2024**, *146*, 31169-31176.

(19) Bai, Y.; Bullard, G.; Olivier, J.-H.; Therien, M. J., Quantitative Evaluation of Optical Free Carrier Generation in Semiconducting Single-Walled Carbon Nanotubes. *J. Am. Chem. Soc.* **2018**, *140*, 14619-14626.

(20) Deria, P.; Von Bargen, C. D.; Olivier, J.-H.; Kumbhar, A. S.; Saven, J. G.; Therien, M. J., Single-handed helical wrapping of single-walled carbon nanotubes by chiral, ionic, semiconducting polymers. *J. Am. Chem. Soc.* **2013**, *135*, 16220-16234.

(21) Von Bargen, C. D.; MacDermaid, C. M.; Lee, O.-S.; Deria, P.; Therien, M. J.; Saven, J. G., Origins of the helical wrapping of phenyleneethynylene polymers about single-walled carbon nanotubes. *J. Phys. Chem. B* **2013**, *117*, 12953-12965.

(22) Mastrocinque, F.; Bullard, G.; Alatis, J. A.; Albro, J. A.; Nayak, A.; Williams, N. X.; Kumbhar, A.; Meikle, H.; Widel, Z. X. W.; Bai, Y.; Harvey, A. K.; Atkin, J. M.; Waldeck, D. H.; Franklin, A. D.; Therien, M. J., Band gap opening of metallic single-walled carbon nanotubes via noncovalent symmetry breaking. *Proc. Natl. Acad. Sci. U.S.A.* **2024**, *121*, e2317078121.

(23) Deria, P.; Olivier, J.-H.; Park, J.; Therien, M. J., Potentiometric, Electronic, and Transient Absorptive Spectroscopic Properties of Oxidized Single-Walled Carbon Nanotubes Helically Wrapped by Ionic, Semiconducting Polymers in Aqueous and Organic Media. *J. Am. Chem. Soc.* **2014**, *136*, 14193-14199.

(24) Kim, T.; Lin, C.; Schultz, J. D.; Young, R. M.; Wasielewski, M. R., π-Stacking-Dependent Vibronic Couplings Drive Excited-State Dynamics in Perylenediimide Assemblies. *J. Am. Chem. Soc.* **2022**, *144*, 11386-11396.

(25) Roznyatovskiy, V. V.; Gardner, D. M.; Eaton, S. W.; Wasielewski, M. R., Radical Anions of Trifluoromethylated Perylene and Naphthalene Imide and Diimide Electron Acceptors. *Org. Lett.* **2014**, *16*, 696-699.

(26) Würthner, F., Perylene bisimide dyes as versatile building blocks for functional supramolecular architectures. *Chem. Commun.* **2004**, 1564-1579.

(27) Huang, C.; Barlow, S.; Marder, S. R., Perylene-3,4,9,10-tetracarboxylic Acid Diimides: Synthesis, Physical Properties, and Use in Organic Electronics. *J. Org. Chem.* **2011**, *76*, 2386-2407.

(28) Marcus, R. A.; Sutin, N., Electron transfers in chemistry and biology. *Biochim. Biophys. Acta, Rev. Bioenerg.* **1985**, *811*, 265-322.

(29) Marcus, R. A., Electrostatic Free Energy and Other Properties of States Having Nonequilibrium Polarization. I. *J. Chem. Phys.* **1956**, *24*, 979-989.

(30) Dresselhaus, M. S.; Dresselhaus, G.; Jorio, A.; Souza Filho, A. G.; Saito, R., Raman spectroscopy on isolated single wall carbon nanotubes. *Carbon* **2002**, *40*, 2043-2061.

(31) Dresselhaus, M. S.; Dresselhaus, G.; Avouris, P., *Carbon Nanotubes Synthesis, Structure, Properties, and Applications*. 1 ed.; Springer Berlin, Heidelberg: 2001.

(32) Sato, K.; Saito, R.; Jiang, J.; Dresselhaus, G.; Dresselhaus, M. S., Discontinuity in the family pattern of single-wall carbon nanotubes. *Phys. Rev. B* **2007**, *76*, 195446.